Sparsity Regularized Nonlinear Inversion for Microwave Imaging

Taskin, U.; Ozdemir, Ozgur

DOI
10.1109/LGRS.2017.2757087

Publication date
2017

Document Version
Final published version

Published in
IEEE Geoscience and Remote Sensing Letters

Sparsity Regularized Nonlinear Inversion for Microwave Imaging

Ulaş Taşkın and Özgür Özdemir

***Abstract*— We present a novel microwave imaging technique for sparse domain imaging applications. In the proposed method, inverse scattering algorithm modified gradient method (MGM) is combined with a fast iterative shrinkage-thresholding algorithm to improve the resolution and robustness of the MGM by enforcing the sparsity in the imaging domain. The numerical experiments show that the proposed method achieves higher resolution and robustness compared with that of classical MGM. For nonsparse domain reconstruction, the wavelet transformation is adopted to convert nonsparse spatial domain into a sparse wavelet coefficient domain. The feasibility of the proposed method in the wavelet domain is demonstrated through the numerical experiments.**

***Index Terms*— Compressive sensing, inverse scattering, microwave imaging, sparsity regularization, wavelet transform.**

I. Introduction

MICROWAVE imaging techniques estimate the electromagnetic properties of unknown targets using transmitted and received microwave signals and have been widely applied in geoscience and remote sensing, nondestructive testing, and medical applications [1]–[4]. Microwave imaging problem belongs to a category of inverse problem, which is a highly nonlinear and ill-posed problem. To tackle the nonlinearity of the problem, Born-type imaging methods linearize the problem within the weak scatterer assumption [5]. For nonweak scatterers, nonlinear inversion algorithms, such as modified gradient method (MGM) and contrast source inversion (CSI), have been developed where the inverse problem is recast as an optimization problem and solve it iteratively [6]–[9].

On the other hand, in order to overcome the numerical instability issues of such ill-posed inverse problems, a compressive sensing framework has been proposed recently by exploiting sparsity approximation [10], [11]. Among sparsity promoted algorithms, Greedy pursuits algorithms search for the most sparse solution within ℓ_0 pseudonorm-based solutions. The orthogonal matching pursuit-based microwave imaging technique is developed to reconstruct scatterers under the Born approximation in [12]. Hard thresholding approaches have been successfully applied to linear inverse scattering techniques in [13] and [14]. Convex relaxation techniques exploit ℓ_1 norm formulation, which yields convex optimization problems, and hence, classical solution techniques can be applied [15]–[17]. One of the most popular techniques in this category is the iterative shrinkage-thresholding algorithm (ISTA) due to its simplicity, and however, it suffers from a slow convergence rate. Recently, the fast ISTA (FISTA) is developed to improve the convergence rate of ISTA while preserving its computational simplicity [18]. The FISTA exploits a specific linear combination of previous two steps to accelerate the convergence rate, and it has not been applied to any microwave imaging technique. Another convex relaxation method that has gained recognition is the Bayesian compressive sensing (BCS) [19], [20]. BCS recasts the minimization problem in the Bayesian framework by using the relevance vector machine. Thresholding-type algorithms have been combined with the linear inversion algorithm Born iterative method for sparse domain reconstructions [16]. Most of the sparsity-based techniques have been applied to linear inversion techniques; to the best of our knowledge, a few works have been devoted to exploit sparsity in nonlinear imaging methods [9], [21], [22].

The sparsity-based approaches have proven to be successful in the improvement of the stability and resolution of classical imaging techniques for sparse imaging domain. However, for nonsparse imaging domain, the sparsity enforcement would severely degrade the performance of reconstruction results. To tackle this problem, wavelet transform has been employed to transfer the nonsparse domain to sparse domain [21]–[24]. In [23] and [24], the BCS technique has been applied to solve a linear inverse problem in the sparse wavelet domain. The nonlinear inversion method CSI has been implemented in the wavelet domain to remedy the ill-posedness of the problem [21], [22]. Beside wavelet transform, total variation compressive sensing framework has also been developed to address the nonsparseness problem in [25].

In this letter, we aim to improve the resolution of nonlinear imaging method MGM for sparse domain applications. To this aim, we combine the sparsity-based approach FISTA with MGM, and we refer to this approach as MGM-FISTA. The classical MGM updates the unknown object function and electric field in the imaging domain iteratively by simultaneous minimization of residual errors in data and state equations. In the proposed approach, the FISTA is applied in each iteration step of the MGM to enforce the sparsity on the object function. It has been demonstrated through the numerical experiments that the MGM-FISTA outperforms the classical MGM on the detection of closely located targets and

Manuscript received August 2, 2017; revised September 13, 2017; accepted September 13, 2017. Date of publication October 13, 2017; date of current version December 4, 2017. *(Corresponding author: Ulaş Taşkın.)*

U. Taşkın is with the Faculty of Applied Sciences, Delft University of Technology, 2628 CJ Delft, The Netherlands (e-mail: u.taskin@tudelft.nl).

Ö. Özdemir is with the Department of Electronic and Telecommunication Engineering, Istanbul Technical University, 34469 Istanbul, Turkey (e-mail: ozdemiroz3@itu.edu.tr).

Color versions of one or more of the figures in this letter are available online at http://ieeexplore.ieee.org.

Digital Object Identifier 10.1109/LGRS.2017.2757087

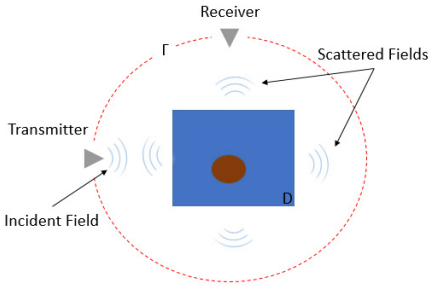

Fig. 1. Geometry of inverse scattering problem.

has improved noise robustness for sparse domain. Moreover, we also exploit the wavelet transformation to extend the application range of the proposed approach to nonsparse domain by transforming nonsparse spatial domain to a sparse wavelet domain. We have shown that by the appropriate choice of the level of wavelet transform, the MGM-FISTA can be successfully applied to nonsparse imaging scenarios.

The outline of this letter is as follows. Section II first describes the formulation of classical MGM and, then, its incorporation with FISTA. Following this, an outline of the MGM-FISTA is explained in both spatial and wavelet domains. In Section III, numerical experiments in sparse and nonsparse domains are presented to assess the performance of the proposed method.

II. Theory

A. Inverse Scattering Algorithm MGM

Consider an unknown scattering object embedded in a homogeneous medium (Fig. 1). We assume that the object in a search domain is irradiated successively by N number of TM polarized incident fields E^i. The scattered field E^s measured on a line Γ enclosing the object can be described by

$$E^s(\mathbf{r}) = k_o^2 \int_D \chi(\mathbf{r}')E^t(\mathbf{r}')G(\mathbf{r},\mathbf{r}')d\mathbf{s}', \quad \mathbf{r} \in \Gamma \tag{1}$$

where k_0 is the wavenumber of the free space and $\chi = \epsilon_r - 1$ is the object function with complex relative permittivity ϵ_r. $\mathbf{r}$ represents the points on the measurement line Γ, $\mathbf{r}'$ represents the points in the imaging domain D, and $\mathbf{ds}'$ is the infinitesimal surface element. $G(\mathbf{r},\mathbf{r}')$ is Green's function of homogeneous medium and given as $G(\mathbf{r},\mathbf{r}') = (i/4H_0^1)(k_0|\mathbf{r}-\mathbf{r}'|)$, where H_0^1 is the zero-order Hankel function of the first kind. The total field E^t in the search domain in (1) can be determined by the following state equation:

$$E^t(\mathbf{r}) = E^i(\mathbf{r}) + k_o^2 \int_D \chi(\mathbf{r}')E^t(\mathbf{r}')G(\mathbf{r},\mathbf{r}')ds', \quad \mathbf{r} \in D. \tag{2}$$

Equations (1) and (2) can be written in more compact operator form

$$E^t = E^i + G_D\chi E^t \tag{3}$$

$$E^s = G_\Gamma \chi E^t. \tag{4}$$

The MGM estimates the unknown object function by simultaneous minimization of residual errors in data and state equations defined in the following cost functional:

$$F(\chi, E^t) = w_\Gamma ||E^s - G_\Gamma \chi E^t||_2^2 + w_D||E^i - E^t + G_D\chi E^t||_2^2 \tag{5}$$

where the normalizing terms w_Γ and w_D are defined as

$$w_\Gamma = \frac{1}{||E^s||_2^2} \quad w_D = \frac{1}{||E^i||_2^2}. \tag{6}$$

Two sequences of object function χ_n and total field E_n^t are defined to minimize cost functional (5) at each iteration step n by the Polak–Ribiere conjugate gradient method

$$E_n^t = E_{n-1}^t + \alpha_n \upsilon_n \tag{7}$$

$$\chi_n = \chi_{n-1} + \beta_n d_n \tag{8}$$

where υ_n and d_n are search directions for total field and object function, respectively. The step sizes α_n and β_n are determined analytically by finding the real root of partial derivative of the cost functional.

The MGM method starts with the initial estimates that are calculated with a backprojection algorithm. Then, the object function and the total field are reconstructed by using the conjugate gradient method steps. In the update of the object function, the total field is considered as a constant with the value of the previous step, and similarly, the object function is considered as a constant with the value of the previous step while updating the total field.

B. Sparsity-Based Algorithm MGM-FISTA

The MGM leads to a smooth reconstruction in a similar manner to ℓ_2 norm regularization, and therefore, it may fail to obtain accurate solutions for sharp edged or closely located sparse objects. In such cases, the MGM can be improved by adding ℓ_1 norm penalty term to the cost function

$$\min_{\chi}\{F(\chi; E^t) + \lambda||\chi||_1\}. \tag{9}$$

The presence of l_1 term forces sparsity in reconstruction. The solution of l_1 norm minimization problem (9) is obtained with incorporation of FISTA and MGM by applying FISTA to object function reconstruction at each step of the MGM iteration.

The FISTA is the improved version of the ISTA, which belongs to the class of forward–backward splitting algorithms [26]. The forward step is line searching with a gradient descent step involving the cost function $F(\chi, E^t)$, and the application of the soft-thresholding operator is the backward step. The computation of the object function at the kth iteration step of the ISTA can be written as

$$\chi^k = H_{\lambda t}(\chi^{k-1} - t^k \nabla F(\chi^{k-1})) \tag{10}$$

where t is the step size and H_δ is the soft-thresholding operator for threshold value δ which is defined as

$$H_\delta(\chi) = \begin{cases} \chi - \delta sign(\chi), & |\chi| > \delta \\ 0, & |\chi| < \delta. \end{cases} \tag{11}$$

In this letter, the threshold value δ is chosen adaptively as starting with initial threshold value and decreasing exponentially in each iteration as $\delta^k = \delta_0 e^{-k\alpha}$. The thresholding parameters,

initial threshold value δ^0, and decay rate α are responsible for resolution of the reconstruction. We use trial and error to determine the optimal thresholding parameters. The optimal value of an initial threshold value is found by sorting the object function vector obtained in the MGM step in a decreasing order and then picking the $T_c/4$th element as δ^0, where T_c is the total number of elements. For α, it is observed that the optimal value lies in the range of $(0, 0.5]$. The FISTA exploits a specific linear combination of previous two values of object function instead of only previous step value to improve the rate of convergence of ISTA [18]

$$\chi_{k+1} = \chi^k + \frac{t^k - 1}{t^{k+1}}(\chi^k - \chi^{k-1}). \tag{12}$$

With this modification, the FISTA outperforms ISTA for the number of iterations to reach the required accuracy. The complete procedure of the proposed method MGM-FISTA is outlined in Algorithm 1.

Algorithm 1 MGM-FISTA Algorithm in Spatial Domain

Input: χ_0, E_0^t
  while $n \leq N_{max}$ **do** *(MGM Loop)*
    Update E_n^t from (7)
    Update χ_n from (8)
    Initialization for FISTA $\chi_n^0 = \chi_n, t^0 = 1, \delta^0 = \chi_n(T_c/4)$
    while $k \leq K_{max}$ **do** *(FISTA Loop)*
      $\delta^k = \delta^0 e^{-k\alpha}$
      $\chi_n^k = H_\delta^k(\chi_n^{k-1} - t^{k-1}\nabla F(\chi_n^{k-1}))$
      $t^{k+1} = \frac{1+\sqrt{1+4(t^k)^2}}{2}$
      $\chi_n^{k+1} = \chi_n^k + \frac{t^k-1}{t^{k+1}}(\chi_n^k - \chi_n^{k-1})$
      $k = k + 1$
    end while
    $n = n + 1$
  end while

C. MGM-FISTA in Wavelet Domain

For nonsparse imaging domain where the target size is comparable with the investigation domain, the sparsity-based algorithm MGM-FISTA cannot yield accurate reconstructions. To tackle this problem, we have employed the wavelet transform to represent object function with a small number of nonzero coefficients without a significant loss of resolution. Wavelet transformation decomposes the object function into different scales with different levels of resolution, and therefore, the number of unknowns can be reduced to a specific level, where the object function of imaging domain can be assumed to be sparse in the wavelet domain.

The operator form of the wavelet transformation of the object function χ can be written as follows:

$$s = \mathcal{W}\chi \tag{13}$$

where $\mathcal{W}$ is the discrete wavelet transform operator and s is the wavelet coefficients. Similarly, inverse discrete wavelet transform $\mathcal{W}^T$ converts the wavelet coefficients back to the spatial coefficients

$$\chi = \mathcal{W}^T s. \tag{14}$$

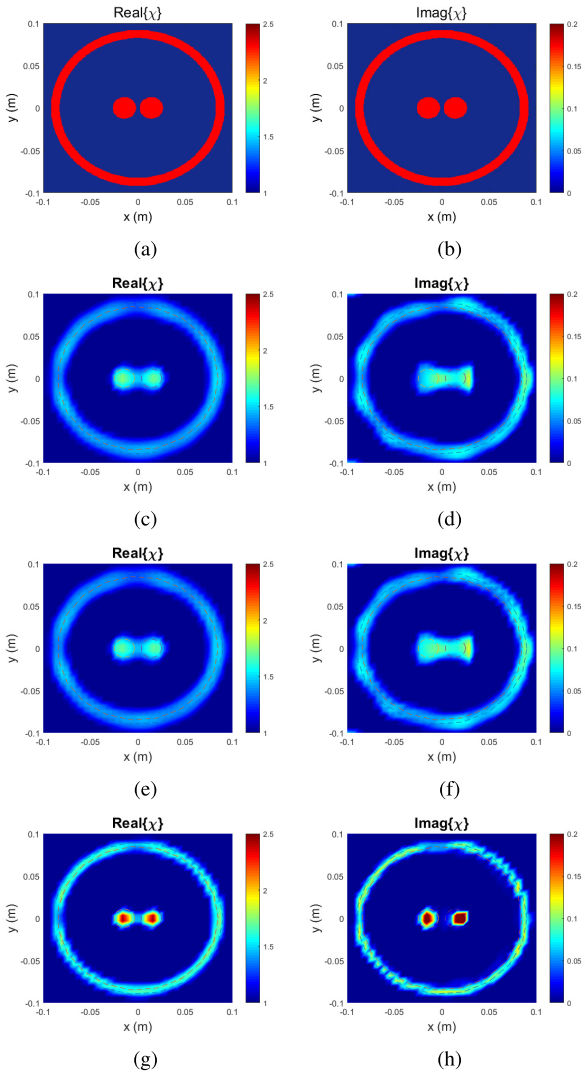

Fig. 2. Reconstruction of sparse domain with noise-free measurement data. Real and imaginary parts of (a) and (b) exact permittivity profile. Reconstructed permittivity profiles by (c) and (d) classical MGM, (e) and (f) MGM-TV, and (g) and (h) MGM-FISTA.

We can write the cost function of minimization problem (5) in the wavelet domain as follows:

$$\min_s \{w_\Gamma ||E^s - G_\Gamma \mathcal{W}^T s E^t||_2^2 + w_D ||E^i - E^t + G_D \mathcal{W}^T s E^t||_2^2 + \lambda ||s||_1\}. \tag{15}$$

In the wavelet domain, the MGM-FISTA defines now two sequences of total field E_n^t (7) and wavelet coefficients s_n. Wavelet coefficients are updated using the conjugate gradient algorithm

$$s_n = s_{n-1} + \beta_n' d_n' \tag{16}$$

where β_n' and d_n' are step size and search directions, respectively. Once the iteration is terminated for predetermined accuracy level or the iteration number, the object function is determined from the wavelet coefficients by inverse transform (14). A summary of the MGM-FISTA in the wavelet domain is given in Algorithm 2.

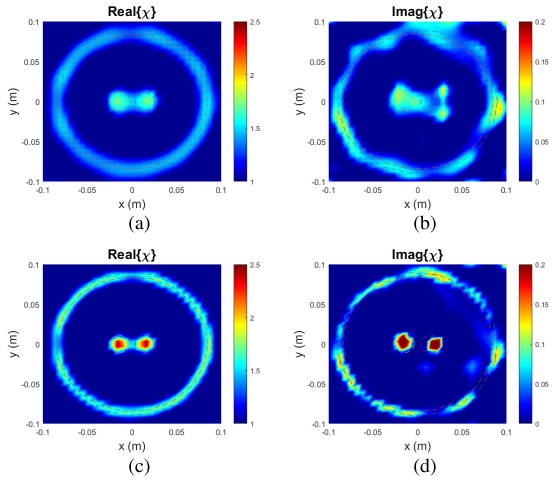

Fig. 3. Reconstruction of sparse domain with noisy data (SNR = 20 dB). Reconstructed real and imaginary part permittivity profiles by (a) and (b) classical MGM and (c) and (d) MGM-FISTA.

Algorithm 2 MGM-FISTA Algorithm in Wavelet Domain

Input: χ_0, E_0^t
$s_0 = \mathcal{W}\chi_0$
while $n \leq N_{max}$ **do** *(MGM Loop)*
Update E_n^t from (7)
Update s_n from (16)
Initialization for FISTA $s_n^0 = s_n, t^0 = 1, \delta^0 = s(T_c/8)$
while $k \leq K_{max}$ **do** *(FISTA Loop)*
$\delta^k = \delta^0 e^{-k\alpha}$
$s_n^k = H_\delta^k(s_n^{k-1} - t^{k-1}\nabla F(s_n^{k-1})$
$t^{k+1} = \frac{1+\sqrt{1+4(t^k)^2}}{2}$
$s_n^{k+1} = s_n^k + \frac{t^k-1}{t^{k+1}}(s_n^k - s_n^{k-1})$
$k = k + 1$
end while
$s_n = s_n^{k+1}$
$\chi_n = \mathcal{W}^T s_n$
$n = n + 1$
end while

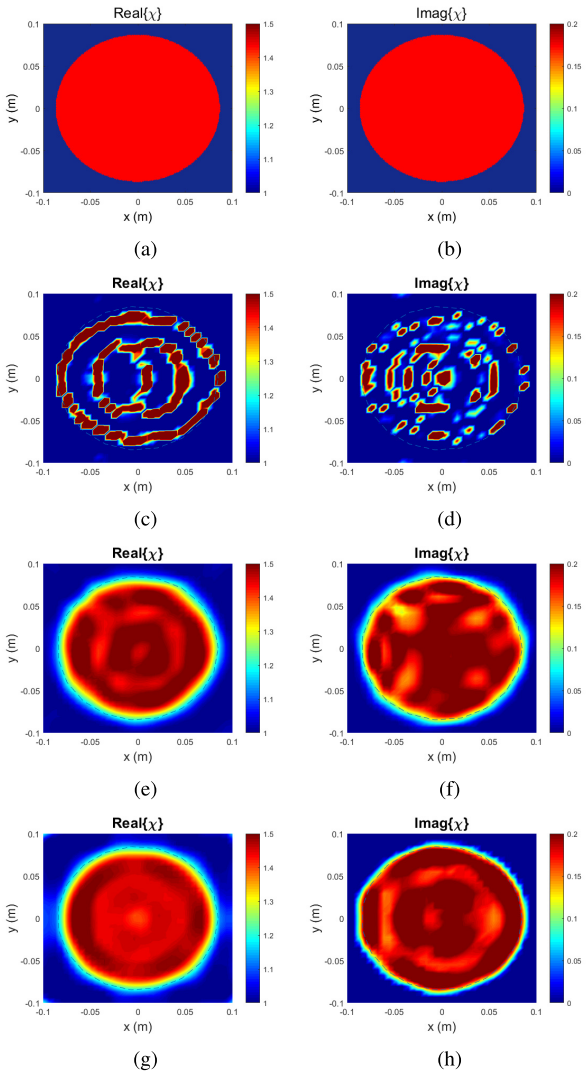

Fig. 4. Reconstruction of nonsparse domain with noisy data (SNR = 37 dB). Real and imaginary parts of (a) and (b) exact permittivity profile. Reconstructed permittivity profiles by (c) and (d) MGM-FISTA in spatial domain, (e) and (f) MGM-FISTA in wavelet domain, and (g) and (h) MGM-TV in spatial domain.

III. Numerical Results

The performance of the proposed method is evaluated using synthetic data generated by the numerical solution of the forward scattering problem. We consider two different imaging domain setups to assess the performance of the method: sparse and nonsparse unknown permittivity distribution in imaging domain. In both setups, 16 transmitter and receiver antennas operated at 3 GHz (a wavelength of 0.1 m) are placed uniformly along the circular line around the search domain. The square-shaped imaging domain has the dimensions of 20 cm × 20 cm, which is discretized into 32 × 32 cells.

A. Sparse Domain Reconstruction

As a first experiment, we compare the performances of the proposed MGM-FISTA with classical MGM and MGM with total variation (MGM-TV) regularization for the sparse permittivity profile, which consists of a circular ring and two closely located circular object given in Fig. 2(a) and (b). The relative permittivity of all objects is chosen as $\varepsilon_r = 2.5 - 0.2i$. In order to quantify how sparse a domain is, a sparsity ratio (S_{ratio}) is defined as the ratio of number of zero elements to the number of all elements of the imaging domain cells, i.e., object matrix: $S_{\text{ratio}} = \text{Nzeros}(\chi)/\text{Ntotal}(\chi)$. The domain can be considered as having sparse representation if the sparsity ratio is close to one. There are 92 nonzero elements among the whole 1024 elements in Fig. 2(a) and (b), which gives $S_{\text{ratio}} = 0.9102$, and hence, it is a sparse domain.

The reconstruction results of real and imaginary parts of permittivity profile are given in Fig. 2, where the dashed line shows the actual boundaries. MGM routine in all algorithms is terminated after 96 iterations. In the MGM-FISTA, the increment in the inner loop iteration increases the computational complexity and has a negligible effect on the result after some point, since the threshold value decreases exponentially in each iteration. In the presented examples, five iteration is found to be optimal value to provide a better resolution while keeping the computational cost as low as possible. As seen in Fig. 2,

while the MGM-FISTA can clearly resolve two circular objects for both real and imaginary parts, MGM and MGM-TV cannot differentiate the two objects, especially in their imaginary part reconstruction. MGM-FISTA also gives better estimates for the permittivity value of the objects. Therefore, we can say that the MGM-FISTA improves the accuracy and spatial resolution of the reconstruction of classical MGM, while TV regularization has no significant effect.

In order to compare the robustness of the methods against noise, random Gaussian noise is added to the measurement data with 20-dB signal-to-noise ratio (SNR). Fig. 3 shows that the reconstructions by MGM are more disrupted by the noise than that of MGM-FISTA.

B. Nonsparse Domain Reconstruction

As a second experiment, we consider a nonsparse profile of the circular object given in Fig. 4(a) and (b). The relative permittivity of the object is chosen as $\varepsilon_r = 1.5 - 0.2i$. There are 540 nonzero elements among the 1024 elements, i.e., $S_{\text{ratio}} = 0.4727$, which indicates the nonsparse imaging domain. When we applied the MGM-FISTA in the spatial domain, it cannot provide an accurate reconstruction, as given in Fig. 4(c) and (d). Then, we applied Daubechies wavelet transform to convert the spatial domain into a sparse wavelet coefficient domain. The sparsity ratio of the imaging domain increases to $S_{\text{ratio}} = 0.87$ with level 4 of wavelet transformation. As it can be seen from Fig. 4(e) and (f), the MGM-FISTA now can provide a quite accurate reconstruction results for such a nonsparse spatial domain. We should note here that the choice of wavelet type and its level is very influential on the performance of the imaging method MGM-FISTA. On the other hand, MGM-TV gives better reconstruction results than MGM-FISTA in spatial domain for nonsparse scenarios [see Fig. 4(g) and (h)].

IV. Conclusion

A novel nonlinear inverse scattering algorithm has been proposed for sparse domain imaging. The cost function in the classical MGM has been modified by adding ℓ_1 norm penalty term in order to enforce sparsity in the minimization scheme. The solution of that cost function is then obtained by combining MGM steps with the soft-thresholding algorithm FISTA. Numerical experiments have been presented to demonstrate the improvement in the accuracy, resolution, and robustness against noise in the proposed method compared with the classical MGM. For nonsparse domain, wavelet transform is applied to convert the nonsparse domain into a sparse one in order to apply MGM-FISTA. It is shown that by appropriate choice of wavelet level, the MGM-FISTA provides successful reconstruction of the nonsparse domain. Future works are devoted to 3-D case applications and the investigation on different methods of sparsification.

References

[1] O. Calla, "Applications of microwave in remote sensing," *Indian J. Radio Space Phys.*, vol. 19, pp. 343–348, Oct./Dec. 1990.

[2] M. Pastorino, "Recent inversion procedures for microwave imaging in biomedical, subsurface detection and nondestructive evaluation applications," *Measurement*, vol. 36, nos. 3–4, pp. 257–269, Oct./Dec. 2004.

[3] S. Kwon and S. Lee, "Recent advances in microwave imaging for breast cancer detection," *Int. J. Biomed. Imag.*, vol. 2016, May 2016, Art. no. 5054912.

[4] R. Chandra, H. Zhou, I. Balasingham, and R. M. Narayanan, "On the opportunities and challenges in microwave medical sensing and imaging," *IEEE Trans. Biomed. Eng.*, vol. 62, no. 7, pp. 1667–1682, Jul. 2015.

[5] Y. M. Wang and W. C. Chew, "An iterative solution of the two-dimensional electromagnetic inverse scattering problem," *Int. J. Imag. Syst. Technol.*, vol. 1, no. 1, pp. 100–108, 1989.

[6] K. Belkebir and A. G. Tijhuis, "Modified2 gradient method and modified Born method for solving a two-dimensional inverse scattering problems," *Inverse Problems*, vol. 17, no. 6, pp. 1671–1688, 2001.

[7] P. M. van den Berg and R. E. Kleinman, "A contrast source inversion method," *Inverse Problems*, vol. 13, no. 6, p. 1607, 1997.

[8] Ö. Özdemir, "Cauchy data contrast source inversion method," *IEEE Geosci. Remote Sens. Lett.*, vol. 11, no. 4, pp. 858–862, Apr. 2014.

[9] A. Desmal and H. Bağcı, "A preconditioned inexact Newton method for nonlinear sparse electromagnetic imaging," *IEEE Geosci. Remote Sens. Lett.*, vol. 12, no. 3, pp. 532–536, Mar. 2015.

[10] D. L. Donoho, "Compressed sensing," *IEEE Trans. Inf. Theory*, vol. 52, no. 4, pp. 1289–1306, Apr. 2006.

[11] A. Massa, "Compressive sensing—Basics, state-of-the-art, and advances in electromagnetic engineering," in *Proc. 9th Eur. Conf. Antennas Propag. (EuCAP)*, May 2015, pp. 1–4.

[12] R. V. Şenyuva, Ö. Özdemir, G. K. Kurt, and E. Anarım, "Electromagnetic imaging of closely spaced objects using matching pursuit based approaches," *IEEE Antennas Wireless Propag. Lett.*, vol. 15, pp. 1179–1182, 2016.

[13] M. Azghani, P. Kosmas, and F. Marvasti, "Microwave medical imaging based on sparsity and an iterative method with adaptive thresholding," *IEEE Trans. Med. Imag.*, vol. 34, no. 2, pp. 357–365, Feb. 2015.

[14] U. Taşkın, E. Yalçın, and Ö. Özdemir, "Hard thresholding based compressed sensing approach for thermoacoustic tomography," in *Proc. URSI Int. Symp. Electromagn. Theory (EMTS)*, Aug. 2016, pp. 815–817.

[15] P. Kosmas and Z. Miao, "Novel inversion tools to improve performance of the DBIM algorithm for microwave medical imaging," in *Proc. IEEE MTT-S Int. Microw. Workshop Ser. RF Wireless Technol. Biomed. Healthcare Appl. (IMWS-Bio)*, Dec. 2014, pp. 1–3.

[16] A. Desmal and H. Bağcı, "Shrinkage-thresholding enhanced born iterative method for solving 2D inverse electromagnetic scattering problem," *IEEE Trans. Antennas Propag.*, vol. 62, no. 7, pp. 3878–3884, Jul. 2014.

[17] P. Shah, U. K. Khankhoje, and M. Moghaddam, "Inverse scattering using a joint $L1-L2$ norm-based regularization," *IEEE Trans. Antennas Propag.*, vol. 64, no. 4, pp. 1373–1384, Apr. 2016.

[18] A. Beck and M. Teboulle, "A fast iterative shrinkage-thresholding algorithm for linear inverse problems," *SIAM J. Imag. Sci.*, vol. 2, no. 1, pp. 183–202, 2009.

[19] G. Oliveri, P. Rocca, and A. Massa, "A Bayesian-compressive-sampling-based inversion for imaging sparse scatterers," *IEEE Trans. Geosci. Remote Sens.*, vol. 49, no. 10, pp. 3993–4006, Oct. 2011.

[20] L. Gharsalli, H. Ayasso, B. Duchêne, and A. Mohammad-Djafari, "Inverse scattering in a Bayesian framework: Application to microwave imaging for breast cancer detection," *Inverse Problems*, vol. 30, no. 11, p. 114011, 2014.

[21] M. Li, O. Semerci, and A. Abubakar, "A contrast source inversion method in the wavelet domain," *Inverse Problems*, vol. 29, no. 2, p. 025015, 2013.

[22] A. B. Ramirez and K. W. A. van Dongen, "Sparsity constrained contrast source inversion," *J. Acoust. Soc. Amer.*, vol. 140, no. 3, pp. 1749–1757, 2016.

[23] L. Guo and A. M. Abbosh, "Microwave imaging of nonsparse domains using born iterative method with wavelet transform and block sparse Bayesian learning," *IEEE Trans. Antennas Propag.*, vol. 63, no. 11, pp. 4877–4888, Nov. 2015.

[24] N. Anselmi, M. Salucci, G. Oliveri, and A. Massa, "Wavelet-based compressive imaging of sparse targets," *IEEE Trans. Antennas Propag.*, vol. 63, no. 11, pp. 4889–4900, Nov. 2015.

[25] G. Oliveri, N. Anselmi, and A. Massa, "Compressive sensing imaging of non-sparse 2D scatterers by a total-variation approach within the born approximation," *IEEE Trans. Antennas Propag.*, vol. 62, no. 10, pp. 5157–5170, Oct. 2014.

[26] P. L. Lions and B. Mercier, "Splitting algorithms for the sum of two nonlinear operators," *SIAM J. Numer. Anal.*, vol. 16, no. 6, pp. 964–979, 1979.